ACS APPLIED MATERIALS & INTERFACES

Research Article

Cite This: ACS Appl. Mater. Interfaces 2018, 10, 21957−21964

www.acsami.org

Design of Nickel-Based Cation-Disordered Rock-Salt Oxides: The Effect of Transition Metal (M = V, Ti, Zr) Substitution in $LiNi_{0.5}M_{0.5}O_2$ Binary Systems

Musa Ali Cambaz,[†] Bhaghavathi P. Vinayan,[†] Holger Euchner,[†,‡] Rune E. Johnsen,[§] Alexander A. Guda,[∥] Andrey Mazilkin,[⊥] Yury V. Rusalev,[∥] Alexander L. Trigub,[#,¶] Axel Gross,[†,‡] and Maximilian Fichtner*[,†,⊥]

[†]Helmholtz Institute Ulm for Electrochemical Energy Storage (HIU), Helmholtzstrasse 11, 89081 Ulm, Germany

[‡]Institute of Theoretical Chemistry, Ulm University, 89069 Ulm, Germany

[§]Department of Energy Conversion and Storage, Technical University of Denmark, Frederiksborgvej 399, 4000 Roskilde, Denmark

[∥]International Research Center "Smart Materials", Southern Federal University, Sladkova 178/24, 344090 Rostov-on-Don, Russia

[⊥]Institute of Nanotechnology, Karlsruhe Institute of Technology (KIT), P.O. Box 3640, 76021 Karlsruhe, Germany

[#]National Research Centre "Kurchatov Institute", 1 Akademika Kurchatova pl., 123098 Moscow, Russia

[¶]Institute of Geology of Ore Deposits (IGEM RAS), 35, Staromonetnyi per., 119017 Moscow, Russia

Supporting Information

ABSTRACT: Cation-disordered oxides have been ignored as positive electrode material for a long time due to structurally limited lithium insertion/extraction capabilities. In this work, a case study is carried out on nickel-based cation-disordered $Fm\bar{3}m$ $LiNi_{0.5}M_{0.5}O_2$ positive electrode materials. The present investigation targets tailoring the electrochemical properties for nickel-based cation-disordered rock-salt by electronic considerations. The compositional space for binary $LiM^{+3}O_2$ with metals active for +3/+4 redox couples is extended to ternary oxides with $LiA_{0.5}B_{0.5}O_2$ with A = Ni^{2+} and B = Ti^{4+}, Zr^{4+}, and V^{+4} to assess the impact of the different transition metals in the isostructural oxides. The direct synthesis of various new unknown ternary nickel-based $Fm\bar{3}m$ cation-disordered rock-salt positive electrode materials is presented with a particular focus on the $LiNi_{0.5}V_{0.5}O_2$ system. This positive electrode material for Li-ion batteries displays an average voltage of ∼2.55 V and a high discharge capacity of 264 $mAhg^{-1}$ corresponding to 0.94 Li. For appropriate cutoff voltages, a long cycle life is achieved. The charge compensation mechanism is probed by XANES, confirming the reversible oxidation and reduction of V^{4+}/V^{5+}. The enhancement in the electrochemical performances within the presented compounds stresses the importance of mixed cation-disordered transition metal oxides with different electronic configuration.

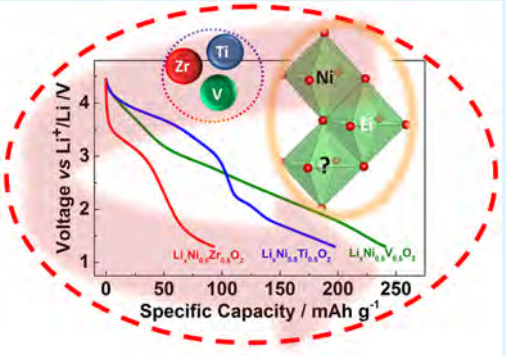

KEYWORDS: *cation-disordered, nickel-based, cathode, lithium-ion battery, mechanochemical synthesis, vanadium*

INTRODUCTION

Currently, the positive electrode is the limiting component that determines energy density, rate capability, and the cost of modern lithium-ion batteries. This results in a strong need for the development of low-cost positive electrode materials with good performance. Among various types of positive electrode materials, research has been primarily focused on well-ordered transition-metal oxide-based cathodes, e.g., layered $LiMO_2$, spinel-like LiM_2O_4, and $Li_2M_2O_4$ systems.[1−3] These material classes are generally regarded as well-performing positive electrode materials as they provide a stable framework structure. This structures provide specific percolating Li sites which are favorable for topotactic insertion and removal of lithium ions. They also enable microscopic diffusion pathways throughout the crystal structure.[4] Having a well-ordered structure with only minor or no cation intermixing that furthermore maintains the structural integrity during operation is considered mandatory to achieve good performance and long cycle life. From the structural point of view, only a few selected systems with distinct chemistries (cobalt containing, except for polyanion-type) have been regarded as suitable candidates, meeting these stringent requirements.[5−7]

Besides this widely investigated class of "well-ordered" materials, there are also other fields for the discovery of novel storage materials. One of these are cation-disordered oxides with rock-salt structure (DRS). These materials have not

Received: February 6, 2018
Accepted: June 4, 2018
Published: June 4, 2018

DOI: 10.1021/acsami.8b02266
ACS Appl. Mater. Interfaces 2018, 10, 21957−21964

received significant attention for a long time because their performance does not match the level of state of the art materials. Furthermore, they have the tendency of being electrochemically inactive, in particular for microsized, well-crystalline particles.[8,9] Here, the random cation distribution hinders sufficient percolation of the Li sites and impedes microscopic diffusion throughout the crystal structure.[10] Hence, cation disorder was anticipated as an inevitable penalty. Recently, and independently from each other, experimental and modeling groups showed that this may not necessarily be the case. Although cation disorder is anticipated as an inevitable penalty, the Ceder[11] group recently delivered a theoretical concept with experimental proof based on percolation theory calculations. These works reveal the hidden potential of Li-rich disordered rock-salt structures. According to this concept, at least 10% lithium excess is necessary to form percolating Li sites in cation-disordered materials to enable microscopic diffusion and high capacities. To the best of our knowledge, all shown examples with high capacity are nanoscale material, which stems from the fact that shorter diffusion pathways are beneficial for kinetically limited systems. Cation-disordered rock-salts are becoming increasingly interesting materials as a consequence of these results.[12−18] The general approach for the rational design of new cation-disordered Li-excess rock-salt phases is the introduction of the Li excess through the formation of solid solutions between stoichiometric cation-disordered $LiMO_2$ and high valent Li-excess compounds such as Li_2MO_3, Li_3MO_4, and Li_4MO_5. This approach is, however, limited by the small number of presently known cation-disordered rock-salt oxides.[19] In this work, we expand this number by working on $LiA_{0.5}B_{0.5}O_2$-based ternary oxides. This provides a broad compositional space to rationally design new materials. This study proposes a practical methodology for the identification of stable cation-disordered rock-salt compounds and their electrochemical and structural characterization. We demonstrate the feasibility of isovalent cation substitution of Ti^{4+} in the well-known cubic compound $LiNi_{0.5}Ti_{0.5}O_2$[20−22] with Zr^{4+} and V^{+4}. To the best of our knowledge, the Zr^{4+} and V^{+4} substituted systems have not been studied as positive electrode material. The effect of the M^{+4} substitution on the $LiNi_{0.5}M_{0.5}O_2$ has been systematically investigated by means of electrochemistry, density functional theory (DFT), and X-ray absorption near edge structure (XANES) spectra with more focus on $LiNi_{0.5}V_{0.5}O_2$ cathode, which promises a good compromise between high capacity and voltage as compared to the other $LiNi_{0.5}M_{0.5}O_2$ with M^{+4} = Zr and Ti.

EXPERIMENTAL SECTION

Synthesis. LNO-M compounds with a formal stoichiometry of $LiNi_{0.5}M_{0.5}O_2$ (M= Zr, Ti, V) were synthesized by high-energy milling of stoichiometric amounts of Li_2O, NiO, and MO_2 with M = Zr, V, and Ti for 20 h using a Fritsch P6 planetary ball mill with 80 mL silicon nitride vial and silicon nitride balls, with a ball to powder ratio of 20:1. All synthesis steps were carried out under inert gas atmosphere (Ar). VO_2 has been synthesized by comproportionation of 1:1 V_2O_3 and V_2O_5.[23] NiO, Li_2O, TiO_2, and ZrO_2 were purchased from Alfa Aesar with a purity ≥99.5%. Only the case of $LiNi_{0.5}V_{0.5}O_2$ is sensitive to air, and moisture and needs to be carefully handled. High temperature treatment of $LiNi_{0.5}V_{0.5}O_2$ results in the formation of an additional spinel phase, which could be due to the charge disproportionation of V^{+4}, which is not further discussed in this work.

Materials Characterizations. Synchrotron X-ray powder diffraction (XRPD) experiments were performed at the Swiss-Norwegian Beamline (SNBL), beamline BM01, at the European Synchrotron Radiation Facility (ESRF). The powdered samples were filled in 0.5 mm quartz capillaries and sealed with wax under an argon atmosphere. XRPD data were collected using a PILATUS 2 M area detector from DECTRIS, a sample-to-detector distance of 142.27 mm, a beamsize of 0.2 × 0.2 mm, a wavelength of 0.68202 Å, a 20° rotation of the capillary, and an exposure time of 20 s. The data were converted to conventional one-dimensional powder patterns using the FIT2D software.[24] In-house X-ray powder diffraction data were collected under rotation of the capillary on a STOE Stadi P diffractometer with Mo Kα1 (λ = 0.7093 Å) using Debye−Scherrer geometry. The powder samples were sealed in quartz capillary (0.5 mm in diameter) under an argon atmosphere.

The X-ray absorption spectra at K-edge of Zr were collected at the beamline "Structural Materials Science"[25] using the equipment of Kurchatov Synchrotron Radiation Source (Moscow, Russia). The storage ring with an electron beam energy of 2.5 GeV and a current of 80−100 mA was used as the source of radiation. All spectra were collected in the transmission mode using a Si (111) channel-cut monochromator. The Ti and V K-edge XANES spectra were recorded using an in-house Rigaku R-XAS spectrometer in transmission mode at room temperature with a crystal monochromator Ge (220) and Ge (311), correspondingly, and at an energy resolution of 0.6 eV, at the Southern Federal University, Russia. Pellets were prepared in a glovebox and sealed in an X-ray transparent bag under an inert atmosphere. An argon-filled ionization chamber (300 mbar pressure) was used to detect the intensity of the X-ray beam before the sample, and a scintillation counter was used for the detection of transmitted intensity. The goniometer section of the spectrometer was filled with helium buffer gas to avoid the air absorption of X-rays. Ten spectra were acquired and averaged for each sample.

Scanning electron microscopy (SEM) and energy dispersive X-ray spectroscopy (EDS) were carried out using the instrument LEO GEMINI 1550 VP equipped with a Silicon Drift Detector (OXFORD Instruments). Transmission electron microscopy (TEM) investigations were performed on a Tecnai F20ST transmission electron microscope operated at 200 kV. Brunauer−Emmett−Teller (BET) surface area analyses of the samples were performed with a Micromeritics ASAP 2020 MP system.

Electrochemical Measurements. Electrochemical tests were carried out in Swagelok-type cell versus lithium metal. Electrode slurries were made of 90 wt % composite and 10 wt % polyviniylidene difluoride (PVDF) binder with *N*-methyl-2-pyrrolidone (NMP) as solvent. The composite consists of active material and Super C65 carbon black in a weight ratio of 80:20. The mixed slurry was coated on an aluminum foil by the doctor blade technique and dried at 120 °C for 12 h under vacuum. Each working electrode (12 mm diameter) contained approximately 3 mg of active material, and Li foil was used as counter electrode. LP30 from BASF (ethylene carbonate/dimethyl carbonate, 1/1 volume ratio with 1 M $LiPF_6$) was used as electrolyte. Cyclic voltammetry (CV) experiments for the cells were carried out from 1.3 to 4.5 V at various scan rates 0.05−1 mVs^{-1} using a Bio-Logic VMP-3 potentiostat at room temperature. Temperature controlled galvanostatic charge−discharge experiments were conducted at 25 °C in climate chambers using an Arbin electrochemical workstation.

Theoretical Calculations. The periodic DFT code VASP[36] was applied for an investigation of stability and electronic structure of different Li_2TMNiO_4 compounds (with TM = Ti, Zr, V). While the PBE functional was used to account for exchange and correlation, the electron−ion interaction was described by the projector augmented wave (PAW) method.[37] Moreover, to take the localization of d-electrons into account, the GGA+U correction was applied for Ni, V, and (Ni 6.0 eV, V 3.1 eV), following the choice of Urban et al.[19,38] To computationally access the disordered rock-salt structure of these compounds, the special quasi random structure approach was applied for the construction of supercells corresponding to the stoichiometry $Li_{16}TM_8Ni_8O_{32}$.

These supercells were optimized with respect to cell volume and atomic positions. For this purpose, a 5 × 5 × 5 k-point mesh, using the Monkhorst−Pack scheme, was chosen in combination with a cutoff energy of 600 eV. In a next step, the structures were delithiated and

DOI: 10.1021/acsami.8b02266
ACS Appl. Mater. Interfaces 2018, 10, 21957−21964

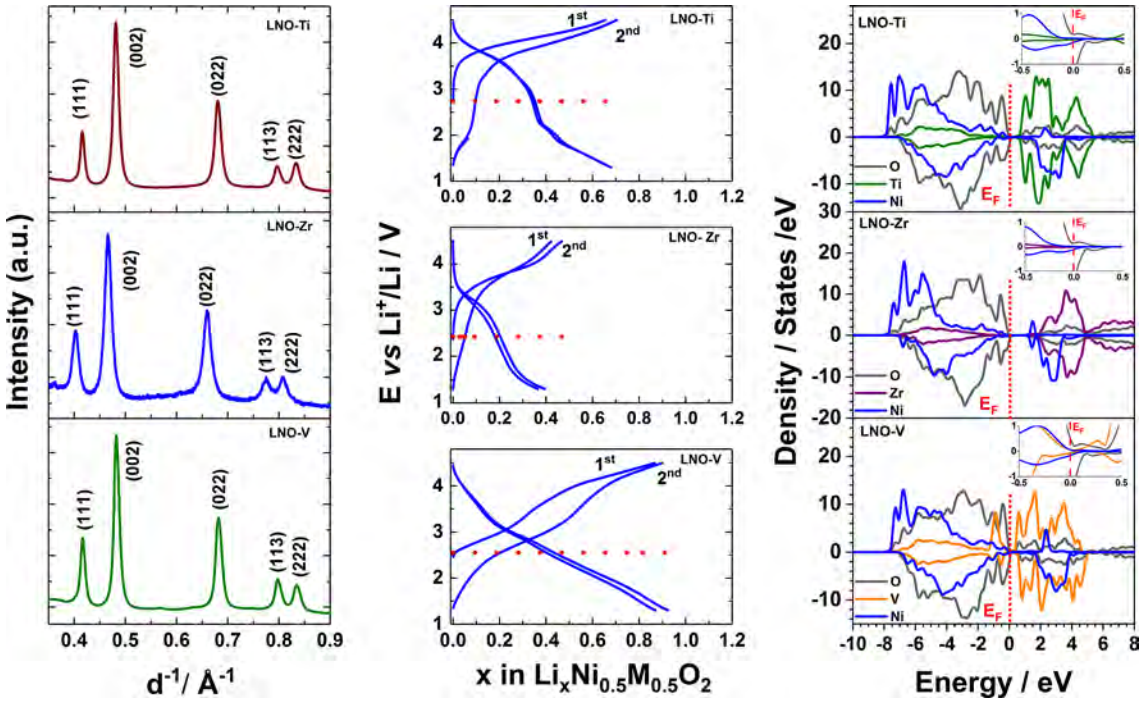

Figure 1. (a) XRPD for LNO-M with M = Ti, Zr, V. (b) Charge−discharge voltage profiles for LNO-M in the voltage range of 4.5−1.3 V at C/20 current rate. (c) Partial density of states (oxygen p- and metal d-states) for LNO-M as obtained from DFT.

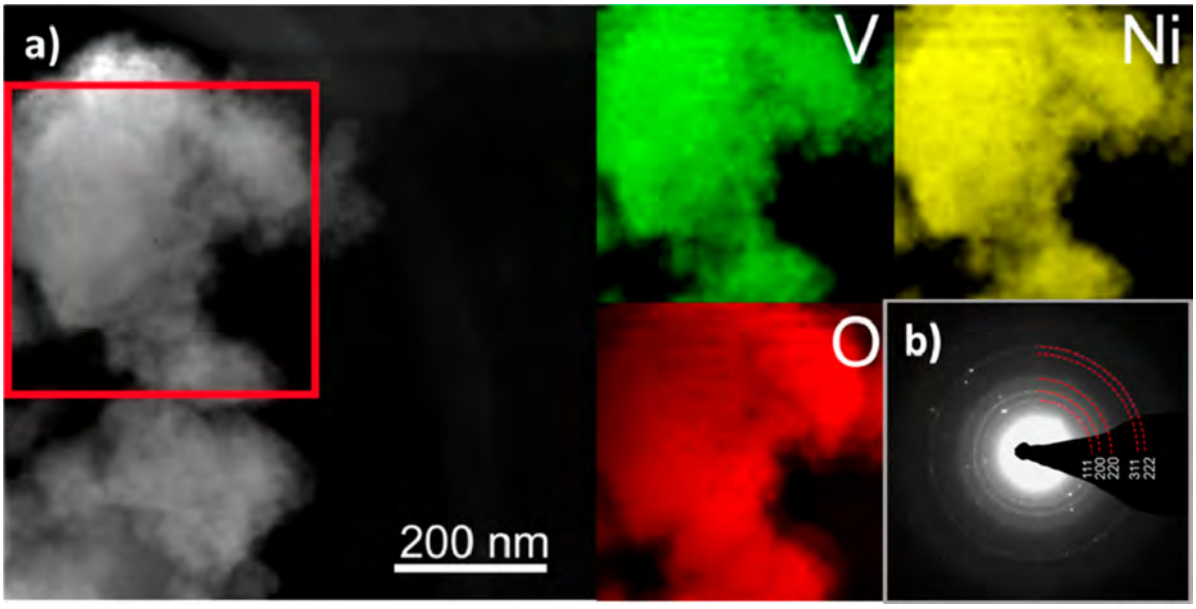

Figure 2. (a) HAADF STEM micrograph and mapping of Ni, V, and O demonstrating the homogeneity of the elemental distribution for LNO-V. (b) SAED patterns of the LNO-V sample. Indexing of the diffraction ring shows rock-salt $Fm\bar{3}m$ structure of LNO-V sample.

also optimized using the same settings. From the total energies of the lithiated and delithiated structures as well as bulk Li, the corresponding average voltage was then calculated.

RESULTS AND DISCUSSION

For comparability reasons all cubic cation-disordered $Li-Ni_{0.5}M_{0.5}O_2$ (LNO-M) with M = Ti^{4+}, Zr^{4+}, V^{4+} were synthesized in the $Fm\bar{3}m$ space group through a direct one-step mechanochemical approach. Cation-disordered rock-salt-like structures were verified for all compositions by XRPD.

Figure 1a shows the XRPD patterns of the LNO-M with M = Ti, Zr, V for the Rietveld refinement shown in the Supporting Information, Figure S1. None of the diffraction patterns contains the characteristic (003) diffraction peak of layered $LiMO_2$ phases with the space group $R\bar{3}m$. Thus, no evidence was found for a layered long-range cation ordering. For a single phase fit with a cubic $Fm\bar{3}m$ symmetry, the lattice constants were estimated as LNO-Ti: a = 4.1551(4) Å, LNO-Zr: a = 4.2780(6) Å, LNO-V: a = 4.1504(5) Å. The elemental mappings of the LNO-M (M = V, Ti, Zr) samples are presented in Figures S2−S4, respectively. Figure 2a shows transmission electron microscopy (TEM) pictures with a corresponding HAADF STEM mapping for LNO-V. This

DOI: 10.1021/acsami.8b02266
ACS Appl. Mater. Interfaces 2018, 10, 21957−21964

Table 1. Average Voltages and Computed Theoretical Voltages for LNO-M

formal stoichiometry	abbreviation	average voltage (V)[a]	theoretical voltage GGA (V)	theoretical voltage GGA+U (V)
$LiNi_{0.5}V_{0.5}O_2$	LNO-V	2.55	2.78	3.44
$LiNi_{0.5}Ti_{0.5}O_2$	LNO-Ti	2.65	3.22	3.90
$LiNi_{0.5}Zr_{0.5}O_2$	LNO-Zr	2.42	3.08	3.70

[a]Average voltage against Li/Li^+ in the cycling range of 4.5−1.3 V.

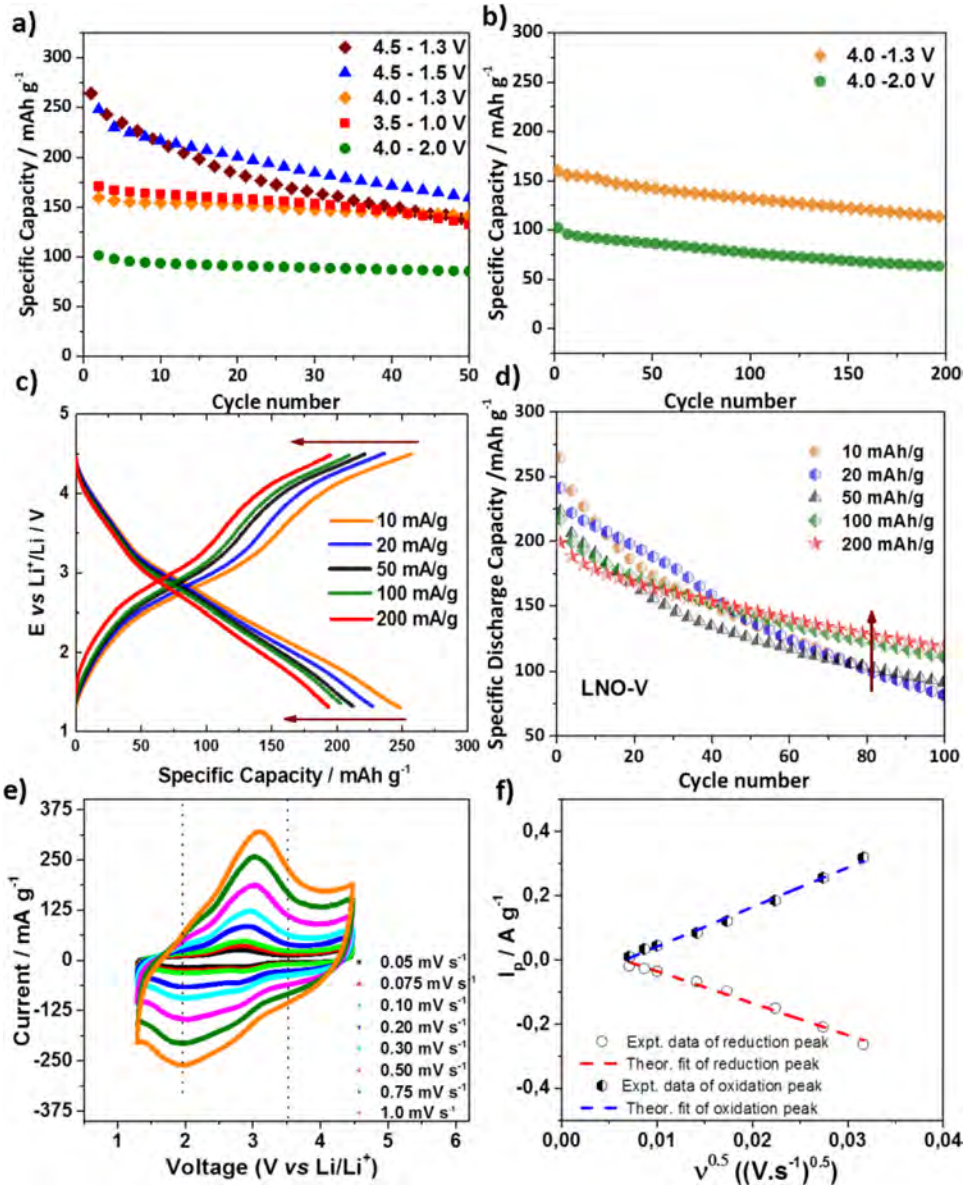

Figure 3. (a) Cycling stability of LNO-V for different cutoff voltages at a current density of 10 mAg^{-1}. (b) Long-term cycling stability of LNO-V for different cutoff voltages at a current density of 10 mAg^{-1}. (c) Charge−discharge voltage profile for LNO-V for different current densities in the range of 4.5−1.3. (d) Cycling stability for LNO-V at different current densities in the voltage range of 4.5−1.3 V. (e) Cyclic voltammograms for LNO-V for various voltage scan rates. (f) LNO-V sample with normalized peak current vs square root of the scan rate.

confirms a homogeneous distribution of Ni and V. The morphology of the particles is representative for mechano-chemically synthesized compounds, showing larger agglomerates with nanocrystalline particles in the range of 20−100 nm. The respective selected area electron diffraction (SAED) pattern is shown in Figure 2b and could be indexed to a cubic $Fm\bar{3}m$ cation-disordered rock-salt phase.

Charge−discharge profiles for LNO-M with M= Ti, Zr, and V are shown in Figure 1b. For a better comparison, the voltage profiles are plotted as a function of lithium content cycled at C/20 rate within the voltage range of 4.5−1.3 V. The plots are stacked vertically to highlight the trends of the distinct redox couples. The cyclic voltammograms in Figure S5 clearly illustrate the oxidation/reduction voltage for all samples. The theoretical capacities calculated on the base of $1e^-$ transfer are given in Table S1. LNO-Zr, Ti, and V show the feasibility to extract 0.47, 0.59, and 0.94 Li in the first charge and insert 0.4, 0.60, and 0.87 Li during discharge, respectively. The observed

DOI: 10.1021/acsami.8b02266
ACS Appl. Mater. Interfaces 2018, 10, 21957−21964

trend is consistent with the understanding that d^0-transition metals do not participate in the redox mechanism as confirmed by the XANES Ti−K and Zr−K edge shown in Figures S6a and b. To gain further understanding of the experimental findings, we conducted DFT calculations to assess the electronic structures of the different materials. The calculated average voltages of the different LNO-M compounds (Table 1) together with additional details on the computational approach are given in the Supporting Information. DFT results qualitatively match to our experiment, see Figure 1b. For d^0 electronic configuration, changing from LNO-Ti to LNO-Zr, the voltage is decreasing. The same trend is observed for d^1 electronic configuration when changing to LNO-V.

For the fully lithiated structures ($LiNi_{0.5}M_{0.5}O_2$ stoichiometry), the electronic density of states (DOS) was calculated, and the corresponding partial DOS for TM d-electrons and oxygen p-electrons was extracted, see Figure 1c. Not surprisingly, the DOS of the group 4 transition metals (TM) (Ti and Zr) containing compounds differ only slightly. There is a dominant contribution of the oxygen p-states close to the Fermi level, which points to a rather limited hybridization of oxygen p- with the Ni d-orbitals. This is indicative for a strong anionic activity, which may result in oxygen release under delithiation.[26] Moreover, for both cases, the d-states of the additional TM (Ti, Zr) are essentially zero from −2 eV to E_F. Only below −2 eV an increased contribution of these d-states is evidenced. By switching from $M^{4+}(d^0)$ for Zr and Ti to $M^{4+}(d^1)$ for V the DOS, however, looks clearly different. For the V compound, significant differences are apparent when compared to the results on group 4 TMs. Interestingly, for the case of $LiNi_{0.5}V_{0.5}O_2$, the Ni pDOS appears quite similar to that of the group 4 TMs. The V spectrum, however, differs strongly from those of Zr or Ti. Indeed, there is a significant contribution of the V d-states close to the Fermi level, so that an oxidation of V before Ni is likely. Here, however, the oxygen p-states are still dominant close to the Fermi level, again indicating anionic activity and possible oxygen release under delithiation.

Owing to the lighter framework structure of LNO-V and the promising electrochemical properties, a deeper investigation has been performed on this particular compound. Cycling stability tests were carried out for different charge/discharge cutoff voltages within the range of 4.5−1.3 V, as shown in Figure 3a. When the cycling voltage is limited to $2.0 \leq x \leq 4.0$ V, the voltage hysteresis is small, as shown in Figure 4. Furthermore, we observe high capacity retention when this cycling window is used, see Figure 3b. However, the small cycling window reduces the reversible capacity, in this case to 160 and 101 mAh g^{-1} for a lower cutoff of x = 1.3 and 2.0 V, respectively. For extended cycling windows, a clear increase in voltage hysteresis can be observed at low and high potentials. This suggests slow kinetics due to bulk diffusion in this region.[27] For the cutoff voltage in the range of 4.5−1.3 V a first discharge capacity of 264 $mAhg^{-1}$ corresponding to 0.92 lithium insertion was observed, yet with a relatively lower capacity retention compared to electrodes with narrower cycling range. The charge/discharge voltage profiles and cyclic stability for LNO-V sample at various current rates (10−200 mAg^{-1}) in the voltage range 4.5−1.3 V are depicted in Figures 3c and d. At higher current densities, an increase in polarization and a decrease in accessible capacity are observed. Moreover, at higher current densities, less capacity fading is observed during cycling. Such irreversibility may occur partly because of side

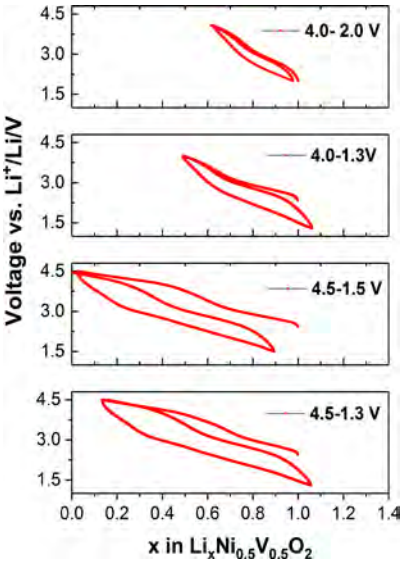

Figure 4. LNO-V charge−discharge profiles for different cutoff voltages at a current density of 10 mAg^{-1}.

reactions with the electrolyte or charged state instability of the material, which was also previously observed for other vanadium-based systems synthesized by the same method.[28,29] The electrode performance can potentially be improved by using electrolyte additives.[30]

To investigate LNO-V kinetics a CV analysis for various scan rates (0.05−1 mVs^{-1}) was performed. In Figure 3e, an increase in the peak current and a separation in oxidation/reduction peaks is observed for higher scan rates. Oxidation/reduction peak currents (I_p) are proportional to the square root of the scan rate (ν) as shown in Figure 3f, which indicates the lithium insertion/extraction is controlled by a semi-infinite linear diffusion process (please see the Supporting Information for detailed study).[31,32] The apparent lithium-ion diffusion coefficients for LNO-V obtained from CV were $\sim 9.5 \times 10^{-16}$ and 6.8×10^{-16} cm^2 s^{-1}, respectively, for the anodic and cathodic reactions.

To assess the reaction mechanism, ex situ XRPD and X-ray absorption spectroscopy (XANES) were applied for LNO-V for different charge/discharged states. The cubic rock-salt structure was maintained during charge/discharge (Figure S8a). For an overlay of the pristine and second charge state LNO-V shown in Figures S8b and c, intensity loss with an increase in background was observed, indicating a partial amorphization, which can manifest itself in a capacity loss and lower Coulombic efficiency due to increased metal dissolution or electrolyte side reactions. Moreover, only a slight peak shift was noticed, and the volume change for lithium insertion/extraction is very low, which is in line with observations for other V containing disordered cubic rock-salt materials.[18,29,33]

Figure 5a shows the Ni K-edge confirming the oxidation state to be +2 for the pristine state. For the charged state, the Ni edge shifts to higher energy and returns back to its starting position after discharge. In the XANES V K-edge spectra of LNO-V (Figure 5b), the pristine state is compared to other V-containing disordered rock-salt compounds, including references like Li_2VO_3 and Li_2VO_2F. LNO-V is showing a similar spectra as Li_2VO_3 with a weak pre-edge located at 5469 eV, which can be attributed to the dipole transition due to p−d hybridization on V in the distorted octahedral environment.[34]

DOI: 10.1021/acsami.8b02266
ACS Appl. Mater. Interfaces 2018, 10, 21957−21964

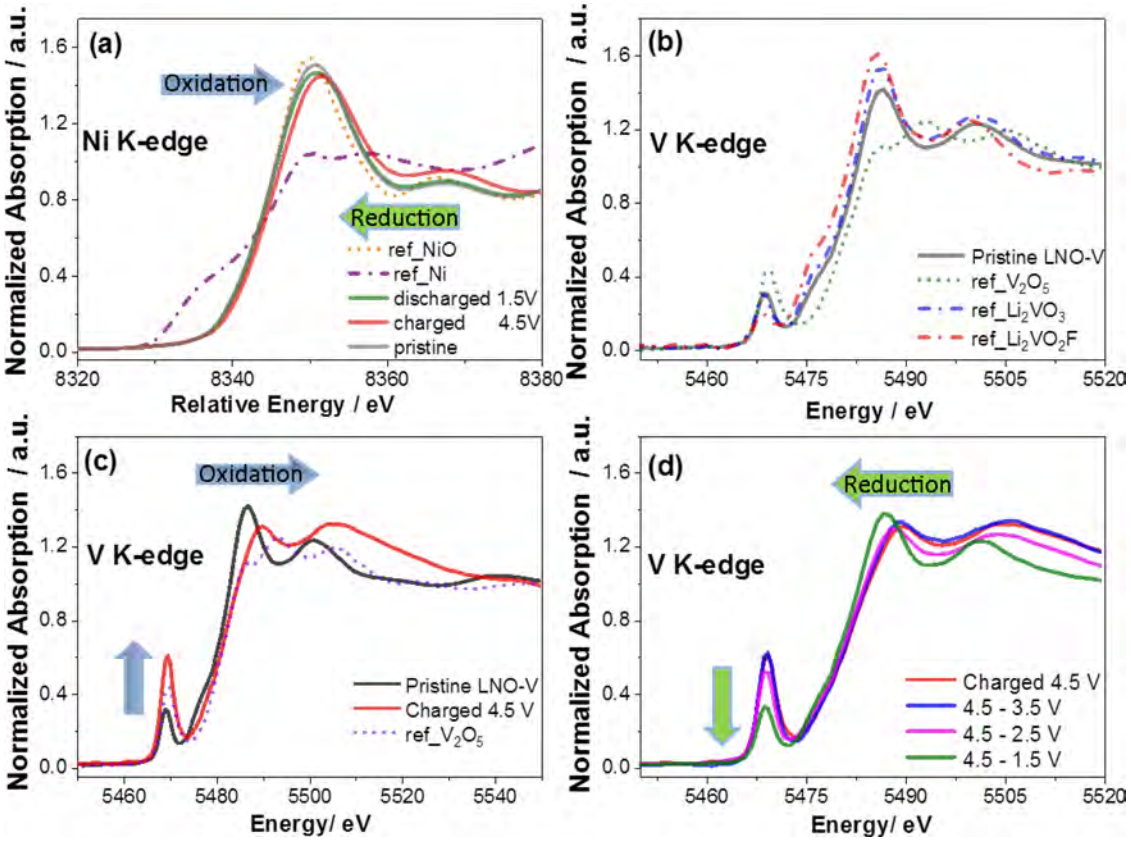

Figure 5. (a) LNO-V change of Ni K-edge during charge−discharge. (b) Comparison of pristine LNO-V with different V containing oxides. (c) LNO-V change of V K-edge during charge. (d) LNO-V change of V K-edge during discharge.

The pre-edge intensity of LNO-V (d^1 with V^{+4}) is higher compared to that of Li_2VO_2F (d^2 with V^{+3}). This can be explained by the lower number of d-electrons and the increased deviation from octahedral symmetry, hinting to a structural distortion of LNO-V. The good agreement between Li_2VO_3 and $LiNi_{0.5}V_{0.5}O_2$ absorption edges confirms the oxidation state of V to be +4. Upon charging, the V absorption edge shifts to the higher energy values close to the values of V_2O_5, as shown in Figure 5c. Thus, the V oxidation state in charged LNO-V is +5. Interesting to note is that the pre-edge peak intensity drastically increases with the oxidation of V. Pre-edge peak intensity is typically increasing with increasing distortion of the octahedral symmetry. Moreover, it changes as a function of the number of d-electrons and is maximized for d^0 configuration.[34] An even stronger pre-edge peak is observed for an inverse spinel $LiNiVO_4$,[35] where V^{5+} exclusively occupies tetrahedral sites. The pre-edge features are consistent with the observation of Yabuuchi et al.,[33] who proposed the partial V^{5+} migration into tetrahedral site and presumably could explain the anomalous small volume changes. The process is highly reversible after discharge to 1.5 V, and the pre-edge peak returns to its original position, as shown in Figure 5c and Figure S9.

The performances of the present materials were compared with state of the art stoichiometric and Li-rich cation-disordered rock-salt oxides in terms of energy density, as shown in Figure 6. More details on the electrochemical performances of the investigated compounds and similar other materials are listed in the Supporting Information, see Tables S2 and S3. The comparison illustrates that the electrochemical performance of the new rock-salt-type compound LNO-V is very promising. The energy density of 682 Wh/kg for the first discharge is comparable to that of many disordered rock-salt oxides considered in literature.

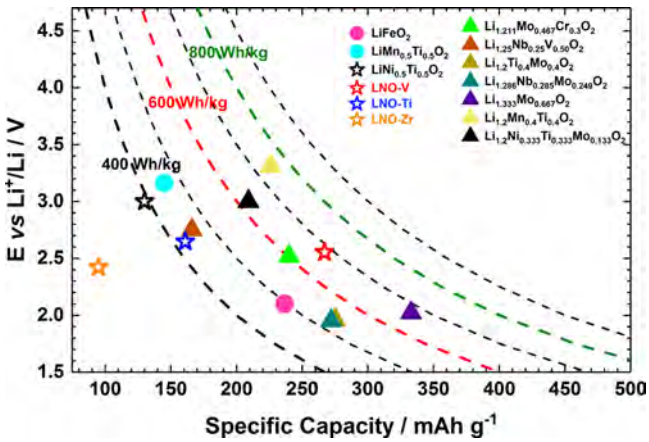

Figure 6. Comparison of various stoichiometric and Li-rich cation-disordered rock-salt oxides with $Fm\bar{3}m$ space group. The --- are isoenergetic lines for specific energy densities (Wh/kg) for different chemistries. Values are taken from the listed compounds in the Supporting Information, Tables S2 and S3.

CONCLUSION

In summary, this study proposes a practical methodology for the design of new cation-disordered rock-salt phases by a mechanochemical approach. We illustrate the feasibility of the complete Ti^{4+} substitution for the $Fm\bar{3}m$ $LiNi_{0.5}Ti_{0.5}O_2$ with Zr

DOI: 10.1021/acsami.8b02266
ACS Appl. Mater. Interfaces 2018, 10, 21957−21964

and V. The effect of the electronic structure for the different transition metals was studied by DFT. Transitioning from $LiNi_{0.5}M_{0.5}O_2$ with M having d^0-configuration for Ti^{4+} and Zr^{4+} to $LiNi_{0.5}M_{0.5}O_2$ with M d^1-configuration with V^{4+} shows considerable improvement in reversible lithium insertion/extraction properties. Among the investigated compounds, $LiNi_{0.5}V_{0.5}O_2$ displays promising electrochemical properties, delivering a capacity of 264 $mAhg^{-1}$ corresponding to 0.92 Li insertion per formula unit. Ex situ XRPD and XANES of the $LiNi_{0.5}V_{0.5}O_2$ reveal a highly reversible V^{4+}/V^{5+} redox process with a slight amorphization upon charge/discharge. This observation is in line with other V-containing cation-disordered rock-salts. This can be associated with the structural distortion during charging indicated by the pre-edge features. The possible origin for these observations could be the partial V^{+5} migration from octahedral to face-shared tetrahedral sites during the charge process. Cation-disordered rock-salt shows interesting electrochemical properties; however, there are remaining challenges and barriers, which have to be addressed in future works. Despite the promise of high capacities, cycling stability with less fading and extended cycling has not yet been demonstrated. Furthermore, undesirable practical drawbacks such as voltage hysteresis and poor rate capability still need to be overcome. The approach used in this work can likely be extended to other ternary compositions and enhance the compositional space for more cation-disordered rock-salt oxides.

■ ASSOCIATED CONTENT

Supporting Information

The Supporting Information is available free of charge on the ACS Publications website at DOI: 10.1021/acsami.8b02266.

XRPD and Rietveld refinement for the compounds, SEM and EDX mapping, cyclic voltammetry curves, XAS Ti and Zr k-edge data, kinetic analysis, adsorption/desorption data, ex situ XRPDS for different SOC, XAS, and V K-edge spectra, table with theoretical values, and table for state of the art cation-disordered rock-salt oxides (PDF)

■ AUTHOR INFORMATION

Corresponding Author

*E-mail: m.fichtner@kit.edu.

ORCID

Musa Ali Cambaz: 0000-0002-4249-3486

Bhaghavathi P. Vinayan: 0000-0001-6491-5160

Axel Gross: 0000-0003-4037-7331

Notes

The authors declare no competing financial interest.

■ ACKNOWLEDGMENTS

Financial support is acknowledged by the FET-OPEN project "LiRichFCC" of the European Commission (Grant 711792). The staff at beamline BM01, SNBL/ESRF, is greatly acknowledged for experimental assistance. The Danish Research Council is acknowledged for financial support in relation to the synchrotron experiments (via DANSCATT). A.A.G. and Y.V.R. acknowledge a grant of the RFBR accoring to the research project No 17-02-01350\17. A.L.T. acknowledges the Ministry of Education and Science of the Russian Federation (Project code RFMEFI61917X0007) for measuring XAS data at Kurchatov Synchrotron Radiation Source. The work was supported by Karlsruhe Nano Micro Facility.

■ REFERENCES

(1) Etacheri, V.; Marom, R.; Elazari, R.; Salitra, G.; Aurbach, D. Challenges in the Development of Advanced Li-Ion Batteries: A Review. *Energy Environ. Sci.* **2011**, *4*, 3243−3262.

(2) Thackeray, M. M. Structural Considerations of Layered and Spinel Lithiated Oxides for Lithium Ion Batteries. *J. Electrochem. Soc.* **1995**, *142*, 2558−2563.

(3) Whittingham, M. S. Lithium Batteries and Cathode Materials. *Chem. Rev.* **2004**, *104*, 4271−4301.

(4) Van Der Ven, A.; Bhattacharya, J.; Belak, A. A. Understanding Li Diffusion in Li-Intercalation Compounds. *Acc. Chem. Res.* **2013**, *46*, 1216−1225.

(5) Rougier, A. Effect of Cobalt Substitution on Cationic Distribution in $LiNi_{1-y}Co_yO_2$ Electrode Materials. *Solid State Ionics* **1996**, *90*, 83−90.

(6) Liu, W.; Oh, P.; Liu, X.; Lee, M. J.; Cho, W.; Chae, S.; Kim, Y.; Cho, J. Nickel-Rich Layered Lithium Transition-Metal Oxide for High-Energy Lithium-Ion Batteries. *Angew. Chem., Int. Ed.* **2015**, *54*, 4440−4457.

(7) Reed, J.; Ceder, G. Role of Electronic Structure in the Susceptibility of Metastable Transition-Metal Oxide Structures to Transformation. *Chem. Rev.* **2004**, *104*, 4513−4533.

(8) Tabuchi, M.; Nakashima, A.; Shigemura, H.; Ado, K.; Kobayashi, H.; Sakaebe, H.; Tatsumi, K.; Kageyama, H.; Nakamura, T.; Kanno, R. Fine $Li_{(4-x)/3}Ti_{(2-2x)/3}Fe_xO_2$($0.18 \leq x \leq 0.67$) Powder with Cubic Rock-Salt Structure as a Positive Electrode Material for Rechargeable Lithium Batteries. *J. Mater. Chem.* **2003**, *13*, 1747−1757.

(9) Li, J.; Li, J.; Luo, J.; Wang, L.; He, X. Recent Advances in the $LiFeO_2$-Based Materials for Li-Ion Batteries. *Int. J. Electrochem. Sci.* **2011**, *6*, 1550−1561.

(10) Urban, A.; Lee, J.; Ceder, G. The Configurational Space of Rocksalt-Type Oxides for High-Capacity Lithium Battery Electrodes. *Adv. Energy Mater.* **2014**, *4*, 1400478.

(11) Lee, J.; Urban, A.; Li, X.; Su, D.; Hautier, G.; Ceder, G. Unlocking the Potential of Cation-Disordered Oxides for Rechargeable Lithium Batteries. *Science* **2014**, *343*, 519−522.

(12) Seo, D.-H.; Lee, J.; Urban, A.; Malik, R.; Kang, S.; Ceder, G. The Structural and Chemical Origin of the Oxygen Redox Activity in Layered and Cation-Disordered Li-Excess Cathode Materials. *Nat. Chem.* **2016**, *8*, 692−697.

(13) Lee, J.; Seo, D.-H.; Balasubramanian, M.; Twu, N.; Li, X.; Ceder, G. A New Class of High Capacity Cation-Disordered Oxides for Rechargeable Lithium Batteries: Li−Ni−Ti−Mo Oxides. *Energy Environ. Sci.* **2015**, *8*, 3255−3265.

(14) Yabuuchi, N.; Takeuchi, M.; Nakayama, M.; Shiiba, H.; Ogawa, M.; Nakayama, K.; Ohta, T.; Endo, D.; Ozaki, T.; Inamasu, T.; et al. High-Capacity Electrode Materials for Rechargeable Lithium Batteries: Li_3NbO_4-Based System with Cation-Disordered Rocksalt Structure. *Proc. Natl. Acad. Sci. U. S. A.* **2015**, *112*, 7650−7655.

(15) Hoshino, S.; Glushenkov, A. M.; Ichikawa, S.; Ozaki, T.; Inamasu, T.; Yabuuchi, N. Reversible Three-Electron Redox Reaction of Mo^{3+}/Mo^{6+} for Rechargeable Lithium Batteries. *ACS Energy Lett.* **2017**, *2*, 733−738.

(16) Yabuuchi, N.; Nakayama, M.; Takeuchi, M.; Komaba, S.; Hashimoto, Y.; Mukai, T.; Shiiba, H.; Sato, K.; Kobayashi, Y.; Nakao, A.; et al. Origin of Stabilization and Destabilization in Solid-State Redox Reaction of Oxide Ions for Lithium-Ion Batteries. *Nat. Commun.* **2016**, *7*, 13814.

(17) Wang, X.; Huang, Y.; Ji, D.; Omenya, F.; Karki, K.; Sallis, S.; Piper, L. F. J.; Wiaderek, K. M.; Chapman, K. W.; Chernova, N. A.; et al. Structure Evolution and Thermal Stability of High-Energy-Density Li-Ion Battery Cathode Li_2VO_2F. *J. Electrochem. Soc.* **2017**, *164*, A1552−A1558.

(18) Dominko, R.; Garrido, C. V. A.; Bele, M.; Kuezma, M.; Arcon, I.; Gaberscek, M. Electrochemical Characteristics of $Li_{2-x}VTiO_4$ Rock Salt Phase in Li-Ion Batteries. *J. Power Sources* **2011**, *196*, 6856−6862.

DOI: 10.1021/acsami.8b02266
ACS Appl. Mater. Interfaces 2018, 10, 21957−21964

(19) Urban, A.; Matts, I.; Abdellahi, A.; Ceder, G. Computational Design and Preparation of Cation-Disordered Oxides for High-Energy-Density Li-Ion Batteries. *Adv. Energy Mater.* **2016**, *6*, 1600488.
(20) Trócoli, R.; Cruz-Yusta, M.; Morales, J.; Santos-Peña, J. On the Limited Electroactivity of Li_2NiTiO_4 Nanoparticles in Lithium Batteries. *Electrochim. Acta* **2013**, *100*, 93−100.
(21) Sebastian, L.; Gopalakrishnan, J. Li_2MTiO_4 (M = Mn, Fe, Co, Ni): New Cation-Disordered Rocksalt Oxides Exhibiting Oxidative Deintercalation of Lithium. Synthesis of an Ordered Li_2NiTiO_4. *J. Solid State Chem.* **2003**, *172*, 171−177.
(22) Küzma, M.; Dominko, R.; Meden, A.; Makovec, D.; Bele, M.; Jamnik, J.; Gaberšček, M. Electrochemical Activity of Li_2FeTiO_4 and Li_2MnTiO_4 as Potential Active Materials for Li Ion Batteries: A Comparison with Li_2NiTiO_4. *J. Power Sources* **2009**, *189*, 81−88.
(23) Brauer, G. *Handbook of Preparative Inorganic Chemistry*; Academic Press: New York, NY, 1965; Vol *144*, p 703.
(24) Hammersley, A. P.; Svensson, S. O.; Hanfland, M.; Fitch, A. N.; Hausermann, D. Two-Dimensional Detector Software: From Real Detector to Idealised Image or Two-Theta Scan. *High Pressure Res.* **1996**, *14*, 235−248.
(25) Chernyshov, A. A.; Veligzhanin, A. A.; Zubavichus, Y. V. Structural Materials Science End-Station at the Kurchatov Synchrotron Radiation Source: Recent Instrumentation Upgrades and Experimental Results. *Nucl. Instrum. Methods Phys. Res., Sect. A* **2009**, *603*, 95−98.
(26) Saubanère, M.; McCalla, E.; Tarascon, J.-M.; Doublet, M.-L. The Intriguing Question of Anionic Redox in High-Energy Density Cathodes for Li-Ion Batteries. *Energy Environ. Sci.* **2016**, *9*, 984−991.
(27) Assat, G.; Delacourt, C.; Corte, D. A. D.; Tarascon, J.-M. Editors' Choice-Practical Assessment of Anionic Redox in Li-Rich Layered Oxide Cathodes: A Mixed Blessing for High Energy Li-Ion Batteries. *J. Electrochem. Soc.* **2016**, *163*, A2965−A2976.
(28) Chen, R.; Ren, S.; Yavuz, M.; Guda, A. A.; Shapovalov, V.; Witter, R.; Fichtner, M.; Hahn, H. Li(+) Intercalation in Isostructural Li_2VO_3 and Li_2VO_2F with O(2-) and Mixed O(2-)/F(−) Anions. *Phys. Chem. Chem. Phys.* **2015**, *17*, 17288−17295.
(29) Chen, R.; Ren, S.; Knapp, M.; Wang, D.; Witter, R.; Fichtner, M.; Hahn, H. Disordered Lithium-Rich Oxyfluoride as a Stable Host for Enhanced Li^+ Intercalation Storage. *Adv. Energy Mater.* **2015**, *5*, 1401814.
(30) Kim, J.; Lee, H.; Cha, H.; Yoon, M.; Park, M.; Cho, J. Prospect and Reality of Ni-Rich Cathode for Commercialization. *Adv. Energy Mater.* **2018**, *8*, 1702028.
(31) Cambaz, M. A.; Anji Reddy, M.; Vinayan, B. P.; Witte, R.; Pohl, A.; Mu, X.; Chakravadhanula, V. S. K.; Kübel, C.; Fichtner, M. Mechanical Milling Assisted Synthesis and Electrochemical Performance of High Capacity $LiFeBO_3$ for Lithium Batteries. *ACS Appl. Mater. Interfaces* **2016**, *8*, 2166−2172.
(32) Zhu, Y.; Wang, C. Novel CV for Phase Transformation Electrodes. *J. Phys. Chem. C* **2011**, *115*, 823−832.
(33) Nakajima, M.; Yabuuchi, N. Lithium-Excess Cation-Disordered Rocksalt-Type Oxide with Nanoscale Phase Segregation: $Li_{1.25}Nb_{0.25}V_{0.5}O_2$. *Chem. Mater.* **2017**, *29*, 6927−6935.
(34) Yamamoto, T. Assignment of Pre-Edge Peaks in K-Edge x-Ray Absorption Spectra of 3d Transition Metal Compounds: Electric Dipole or Quadrupole? *X-Ray Spectrom.* **2008**, *37*, 572−584.
(35) Liu, R. S.; Cheng, Y. C.; Gundakaram, R.; Jang, L. Y. Crystal and Electronic Structures of Inverse Spinel-Type $LiNiVO_4$. *Mater. Res. Bull.* **2001**, *36*, 1479−1486.
(36) Kresse, G.; Furthmüller, J. Efficient iterative schemes for ab initio total-energy calculations using a plane-wave basis set. *Phys. Rev. B: Condens. Matter Mater. Phys.* **1996**, *54*, 11169.
(37) Kresse, G.; Joubert, D. From ultrasoft pseudopotentials to the projector augmented-wave method. *Phys. Rev. B: Condens. Matter Mater. Phys.* **1999**, *59*, 1758−1775.
(38) Zunger, Z.; Wei, S.-H.; Ferreira, L. G.; Bernard, J. E. Special quasirandom structures. *Phys. Rev. Lett.* **1990**, *65*, 353.

DOI: 10.1021/acsami.8b02266
ACS Appl. Mater. Interfaces 2018, 10, 21957−21964